DOI: 10.61782/fa.2023.0599

forum acusticum 2023

PROBABILISTIC ESTIMATION OF THE OBLIQUE INCIDENCE SOUND ABSORPTION COEFFICIENT - A NUMERICAL CONCEPT STUDY

Martin Eser[1*] **Caglar Gurbuz**[1] **Eric Brandão**[2]
Steffen Marburg[1]

[1] Chair of Vibroacoustics of Vehicles and Machines, Technical University of Munich, Germany
[2] Acoustical Engineering, Federal University of Santa Maria, Brazil

ABSTRACT

The *in situ* absorption characteristics of sound absorbing panels can be inversely estimated from sound field measurements above a specimen under free-field conditions or in a semi-anechoic chamber. In any case, the measurement and the inference process are subject to numerous sources of uncertainty. In this contribution, a Bayesian approach is applied to assess the uncertain, frequency-dependent material properties (complex-valued wavenumber and density) of a layer made of melamine foam. In the initial phase of inference, the quantities are inferred at a discrete frequency based on a diffuse prior. In the sequential phase, the posterior mean at an analyzed frequency serves as the prior mean at the subsequent frequency. The uncertain oblique plane wave incidence absorption coefficient then follows from the identified material properties. A virtual source antenna, modeled as a single monopole source, which is sequentially moved parallel to the specimen's surface, is used to excite the sound field and a combined pressure-particle velocity probe records the specific impedance above the specimen. We demonstrate the application of the framework for simulated noisy measurements in a semi-anechoic chamber and assess the uncertain material properties and the absorption coefficient.

Keywords: *bayesian inference, oblique incidence sound absorption, acoustic material characterization, uncertainty quantification.*

**Corresponding author*: *m.eser@tum.de.*

1. INTRODUCTION

The normal incidence plane wave sound absorption coefficient is most commonly determined by using standardized impedance tube techniques, *e.g.* ISO 10534–2 [1]. However, the absorption coefficient of a sound absorbing panel *in situ* can vary significantly with frequency and the angle of incidence of incoming sound waves [2]. The inverse characterization of sound absorbing panels based on impedance measurements under free-field conditions, *e.g.* in a semi-anechoic chamber, is a viable technique to estimate the oblique incidence sound absorption coefficient [3]. The experimental setups used for such measurements vary in the number of sound sources and the number of receivers, *cf.* Refs. [3–5]. However, there are numerous sources of uncertainty associated with such impedance measurements [6]. This paper aims at quantifying the uncertainty in an estimate of the oblique incidence sound absorption coefficient. For this purpose, a Bayesian framework is adopted to directly infer the frequency-dependent sound propagation characteristics of a panel absorber. A virtual source antenna serves to excite the sound field and a single combined sound pressure-particle velocity probe (PU-probe) is used to record the sound field above the sample under investigation.

2. THEORY

The sample under investigation is a flat panel absorber made of a single layer of melamine foam. This porous layer is modeled as an equivalent fluid layer, which is characterized with the unknown sound propagation characteristics, *i.e.* the complex-valued wavenumber k_p and effective density ρ_p. An inverse problem, based on measurements of the specific impedance above the panel, needs to be solved to retrieve these sound propagation

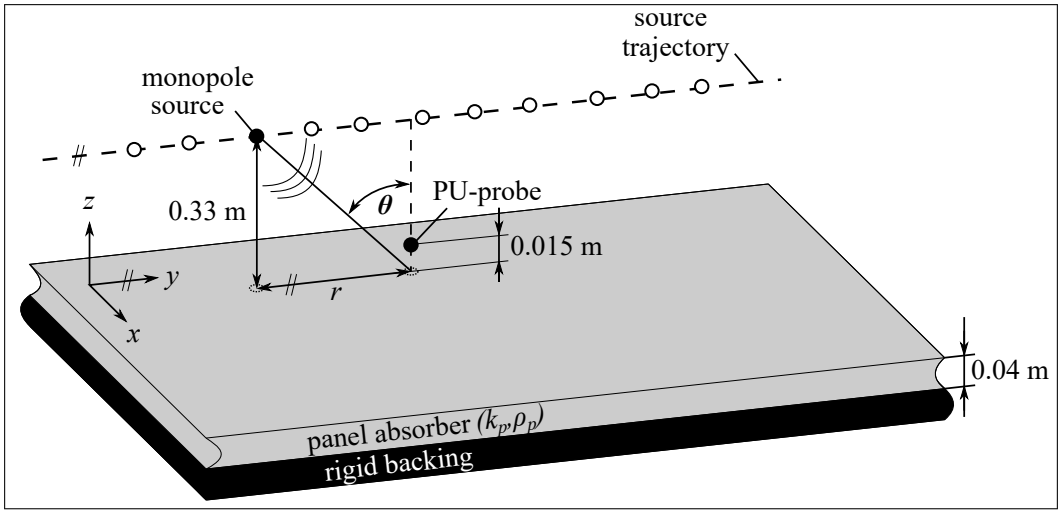

Figure 1. Schematic setup of the impedance measurement above a flat panel absorber using a virtual source antenna and a combined sound pressure-particle velocity probe (PU-probe).

characteristics.

Fig. 1 schematically shows the setup for the free-field impedance measurement above the panel. The PU-probe's position is given by $\mathbf{r} = (x_\mathrm{r} = 0, y_\mathrm{r} = 0, z_\mathrm{r} = 0.015)$ m. For the virtual source antenna, a single monopole source is positioned at $\mathbf{r}_\mathrm{s} = (x_\mathrm{s} = 0, y_\mathrm{s}, z_\mathrm{s} = 0.33)$ m and y_s is varied, such that the source is sequentially moved parallel to the panel's surface following the source trajectory. The specific impedance, *i.e.* the ratio of the sound pressure and the particle velocity perpendicular to the panel's surface, is recorded by the PU-probe for each position of the sound source. For modeling the sound field, we assume a harmonic time dependence of $\exp(+\mathrm{i}\omega t)$, where $\mathrm{i}^2 = -1$, is the imaginary unit, $\omega = 2\pi f$, is the angular frequency at the frequency f and t is the time. Hence, the recorded sound pressure $p(\mathbf{r}, \mathbf{r}_\mathrm{S})$ is directly proportional to the specific half-space Green's function [7]

$$G(\mathbf{r}, \mathbf{r}_\mathrm{s}) = \frac{\exp(-\mathrm{i}k_\mathrm{a}D_0)}{D_0} + \\ +\mathrm{i}\int_0^\infty \tilde{R}(k_r)\,\frac{\exp(\mathrm{i}k_{z,\mathrm{a}}(z_\mathrm{r}+z_\mathrm{s}))}{k_{z,\mathrm{a}}}\,k_r J_0(k_r r)\,\mathrm{d}k_r, \quad (1)$$

where $r = \sqrt{(x_\mathrm{r}-x_\mathrm{s})^2 + (y_\mathrm{r}-y_\mathrm{s})^2}$ is the radial distance and $D_0 = \sqrt{r^2 + (z_\mathrm{r}-z_\mathrm{s})^2}$ the total direct distance between the source and the receiver. The wavenumber in the air above the panel is denoted by $k_\mathrm{a} = \omega/c_\mathrm{a}$, where the air above the panel is characterized with the speed of sound $c_\mathrm{a} = 343.4$ m/s and the mass density $\rho_\mathrm{a} = 1.2$ kg/m^3. The vertical wavenumber in air is

$$k_{z,\mathrm{a}} = +\sqrt{k_\mathrm{a}^2 - k_r^2}, \quad (2)$$

where k_r is the radial wavenumber, which serves as the integration variable in Eq. (1). The zeroth order Bessel function is denoted by J_0. The scattered sound field depends on the plane wave reflection coefficient $\tilde{R}(k_r)$, which is given by [8]

$$\tilde{R}(k_r) = \frac{\left(\frac{\mathrm{i}k_{z,\mathrm{a}}}{\rho_\mathrm{a}}\right) - \left(\frac{\mathrm{i}k_{z,\mathrm{p}}}{\rho_\mathrm{p}}\right)\tan(k_{z,\mathrm{p}}d)}{\left(\frac{\mathrm{i}k_{z,\mathrm{a}}}{\rho_\mathrm{a}}\right) + \left(\frac{\mathrm{i}k_{z,\mathrm{p}}}{\rho_\mathrm{p}}\right)\tan(k_{z,\mathrm{p}}d)} \quad (3)$$

for a non-locally reacting layer of finite thickness d. In this study, the thickness of the panel is $d = 0.04$ m. The vertical wavenumber in the panel is given by

$$k_{z,\mathrm{p}} = +\sqrt{k_\mathrm{p}^2 - k_r^2}. \quad (4)$$

The sound field is mathematically challenging to evaluate, due to the integrand in the Green's function [3, 7, 9]. For this reason, the identification of the sound propagation characteristics requires an iterative approach [3]. Once the sound propagation characteristics have been inferred, the oblique incidence plane wave sound absorption coefficient is calculated by [10]

$$\alpha(\theta) = 1 - \left|\frac{Z_\mathrm{s}(\theta)\cos\theta - \rho_\mathrm{a}c_\mathrm{a}}{Z_\mathrm{s}(\theta)\cos\theta + \rho_\mathrm{a}c_\mathrm{a}}\right|^2, \quad (5)$$

for any angle of incidence θ. Here, the surface impedance of the panel Z_s is calculated from the inferred sound propagation characteristics according to [10]

$$Z_\mathrm{s}(\theta) = -\mathrm{i}Z_\mathrm{c}\frac{k_\mathrm{p}\cot\left(d\sqrt{k_\mathrm{p}^2 - k_\mathrm{a}^2\sin^2\theta}\right)}{\phi\sqrt{k_\mathrm{p}^2 - k_\mathrm{a}^2\sin^2\theta}}, \quad (6)$$

where $Z_\mathrm{c} = \omega\phi\rho_\mathrm{p}/k_\mathrm{p}$ is the melamine foam's characteristic impedance and $\phi = 0.99$ is the sample's open porosity.

3. METHODS

We adopt a Bayesian approach, which has initially been proposed for the direct identification of a porous panel absorber's frequency-dependent surface admittance [6]. In this study however, this Bayesian approach is extended to identify the frequency-dependent sound propagation characteristics and the associated uncertainty in these parameters. Note that the inference is not directly conducted for the wavenumber and the effective density, but for their normalized counterparts, *i.e.* the refraction index

$$n = \frac{k_\mathrm{p}}{k_\mathrm{a}} \quad (7)$$

and the ratio of mass density

$$m = \frac{\rho_\mathrm{a}}{\rho_\mathrm{p}}. \quad (8)$$

This favors the inference, since the normalization limits the values of the majority of the sought parameters.

The basic principle for this Bayesian material characterization relies on updating a prior state of knowledge on the normalized sound propagation characteristics – the prior probability – by incorporating the measured specific impedances using a likelihood function. The updated, *i.e.* the posterior, probability on the normalized sound propagation characteristics follows from the product of the prior and the likelihood. We apply sampling-based algorithms to explore the posterior. By doing so, the theoretical sound field, given by Eqs. (1)–(4), needs to be evaluated numerous times for each source-receiver combination in order to evaluate the likelihood. Allard *et al.* [9] have presented a mathematically exact solution for this sound field problem, which can be solved by using numerical integration. However, this approach requires an individual numerical integration for the sound pressure and for the particle velocity for each source-receiver combination, which makes it impractical for the present inverse problem. Therefore, we use the direct discrete complex image method (dDCIM) [7] to efficiently evaluate an accurate approximation of the theoretical sound field. The dDCIM's efficiency is based on a single step solution of the sound field for an arbitrary number of source-receiver combinations, since the coefficients of the complex images are independent of the positions of source and receiver [7].

In general, the posterior probability on the normalized sound propagation characteristics is inferred sequentially for discrete frequencies. However, the computational effort per discrete frequency is reduced by adopting the sequential frequency transfer scheme, which has been proposed in Ref. [6]. The principle of the Bayesian approach with sequential frequency transfer is sketched in Fig. 2 for a single quantity of interest. At first, the posterior probability on the sound propagation characteristics is inferred at the initial frequency f_init based on a diffuse prior, which assigns equal probability to all possible values of the quantity of interest. According to the principle of maximum entropy, we assign uniform prior probabilities to the quantities of interest at the initial frequency, *i.e.*

$$\begin{aligned}
\Re\{n\} &\sim \mathcal{U}(1.0, 3.0), \\
\Im\{n\} &\sim \mathcal{U}(-3.0, 0.0), \\
\Re\{m\} &\sim \mathcal{U}(0.0, 1.0), \\
\Im\{m\} &\sim \mathcal{U}(0.0, 1.0).
\end{aligned}$$

For the refraction index, the lower bound of the real part and the upper bound of the imaginary part are prescribed due to physical constraints associated with the sound propagation in a layer of porous material modeled as an equivalent fluid. The limitation of the refraction index' real part to 1.0 (lower bound) is given by the fact that sound waves generally propagate slower inside the porous panel than in the surrounding air [10]. The restriction of the refraction index' imaginary part to the negative half-space is due to the harmonic time dependence of $\exp(+\mathrm{i}\omega t)$ [10]. The other two bounds of the refraction index are manually set. These bounds need to be cautiously set, since too strict bounds may exclude the correct values for the quantity of interest. As such, the user requires either some experience for setting these bounds or has to adjust them iteratively after inspecting the inference's results. Concerning the ratio of mass density, the bounds of the specified prior are also prescribed due to physical constraints. The air-saturated porous material is heavier than pure air, which limits the parameter range for the real part of the ratio of mass density to the interval

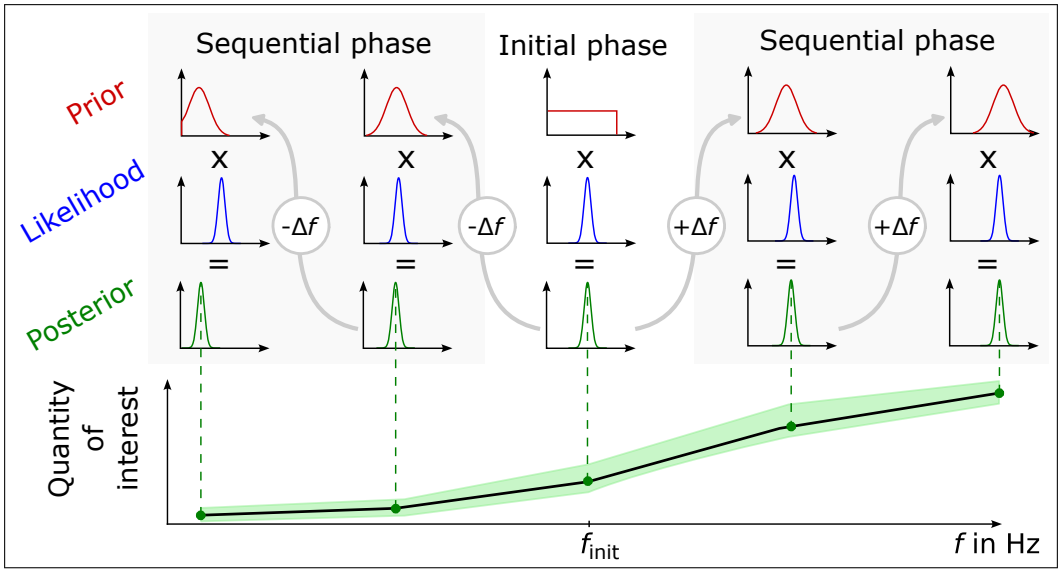

Figure 2. Process scheme of the Bayesian inverse material characterization with sequential frequency transfer. The inference process starts at the initial frequency f_{init} using a diffuse prior. In the sequential phase, the posterior mean at one frequency serves as the prior mean at the subsequent frequency at either $+\Delta f$ or $-\Delta f$.

$[0.0, 1.0]$. Since the imaginary part of the effective density is also limited to the negative half-space due to the harmonic time dependence of $\exp(+\mathrm{i}\omega t)$, the imaginary part of the ratio of mass density is limited to the positive half-space. However, the upper limit of the imaginary part of the ratio of mass density also needs to be cautiously set. Again, the user requires some experience with the material under investigation, but this parameter's range is generally less volatile than for the refraction index.

In the sequential phase, *i.e.* for all remaining frequencies in the frequency range of interest, the procedure follows a hidden Markov chain-like principle, where information of the posterior at one frequency is transferred to the prior at the subsequent frequency. In particular, the posterior mean $\hat{\mu}$ at one frequency serves as the prior mean at the next frequency. As such, this enhanced level of information is directly included in the specification of the prior in the sequential phase, where we assign truncated normal distributions to the quantities of interest, such that

$$
\begin{aligned}
\Re\{n\} &\sim \mathcal{N}_{1.0}^{3.0}\left(\hat{\mu}_{\Re\{n\}}, 0.3\right), \\
\Im\{n\} &\sim \mathcal{N}_{-3.0}^{0.0}\left(\hat{\mu}_{\Im\{n\}}, 0.3\right), \\
\Re\{m\} &\sim \mathcal{N}_{0.0}^{1.0}\left(\hat{\mu}_{\Re\{m\}}, 0.1\right), \\
\Im\{m\} &\sim \mathcal{N}_{0.0}^{1.0}\left(\hat{\mu}_{\Im\{m\}}, 0.1\right).
\end{aligned}
$$

Here, the superscript and subscript indicate the upper and lower bounds of the truncated normal distribution. These bounds are the same as for the specification of the uniform priors at the initial phase. Note that the standard deviation of each truncated normal distribution is set to a fixed value. In this concept study, we have set the standard deviation of the refraction index to 0.3 and to 0.1 for the ratio of mass density. These values have proven to yield sufficient flexibility for the inference framework. In summary, the sequential frequency transfer allows for a more efficient inference at the subsequent frequency since the inference starts in a region of high probability [6].

This concept study is based on simulated impedance measurements under free-field conditions in the frequency range of 100–5000 Hz. This frequency range is chosen here since the layer under investigation exhibits all possible states of sound absorption: starting from nearly no absorption at very low frequencies to maximum absorption at higher frequencies. For the simulated experiments, the specific impedance at the PU-probe's position is evaluated for eleven source positions using the theoretical model proposed by Allard *et al.* [9]. The source positions are evenly spaced along the source trajectory in the interval $y_{\text{s}} \in [-0.33, 0.33]$ m. Hence, the spherical sound waves impinge the panel at angles of incidence

of $\theta \in [-45°, +45°]$. Note that the specific impedances recorded in this simulated experiment contain redundant information due to the radial symmetry of the theoretical sound field model and the evenly spaced source positions. To mimic real measurements, the specific impedances are perturbed by adding Gaussian noise with a constant standard deviation of 0.01. The bias due to the measurement error counterbalances the redundancy in the observations to some extent and is necessary for quantifying the uncertainty. However, the constant magnitude of the noise idealizes the measurement setup to some extent since varying signal-to-noise ratios are expected for real measurements. For example, the simulated experiment assumes a perfectly omnidirectional microphone, while the PU-probe's particle velocity sensor is assumed to be perfectly directional perpendicular to the panel absorber's surface. However, this is not the case in real applications. While real microphones can be considered well omnidirectional up to 5000 Hz, the particle velocity sensor possesses a dipole directional pattern and hence varies with the angle of incidence, depending on its orientation [11].

Concerning the inference process, four individual Markov chains are sampled at each discrete frequency to track the convergence of the results. For the initial phase, the initial frequency is set to $f_{\text{init}} = 1200$ Hz. Here, the Slice sampling algorithm [12] is applied to explore the posterior using 5000 samples and another 1500 burn-in samples per chain. In the sequential phase, all subsequent inferences for lower as well as for higher frequencies are conducted in steps of $\Delta f = 100$ Hz. In this phase, the Sequential Monte Carlo (SMC) sampling approach [13] with 2000 samples per chain is applied to explore the posterior. We change the sampling algorithm between the phases since SMC has shown a better convergence at the subsequent frequencies, where fewer samples are drawn due to the increased level of informativeness of the prior. For the post-processing, the inferred normalized sound propagation properties are transformed back to their dimensional counterparts by using Eqs. (7) and (8).

4. RESULTS

Fig. 3 shows the mean of the wavenumber's posterior probability density, its corresponding 95 % highest density interval (HDI), and the ground truth used for the simulated experiments. Similarly, Fig. 4 shows the mean of the effective density's posterior probability density, its corresponding 95 % HDI, and the ground truth. All approximated frequency-sweeps of the sound propagation characteristics, *i.e.* their means, agree very well with the ground truth, except at 100 Hz. The reason for this is that the wavelength is significantly larger than the layer's thickness at low frequencies, and the particle velocity perpendicular to the panel absorber's surface tends to zero, reproducing the behavior of the sound hard backing. Thus, nearly no sound absorption occurs at these frequencies, and the PU-probe records unreasonably high values for the specific impedance. This renders the inference particularly challenging for low frequencies. The uncertainty in the sound propagation characteristics decreases for frequencies above the initial frequency of 1200 Hz. This is due to the fact that the signal-to-noise ratio is higher for frequencies above 1200 Hz, which is a direct consequence of the frequency-independent, constant noise that has been added to the ground truth of the specific impedance to mimic simulated measurements. The uncertainty increases for frequencies below the initial frequency, in particular for the effective density, which is caused by the lower signal-to-noise ratio in this frequency range. Estimating the real part of the effective density exhibits the most significant uncertainty relative to its true value. This might be caused by the relatively low magnitude of the effective density's real part compared to all other quantities of interest.

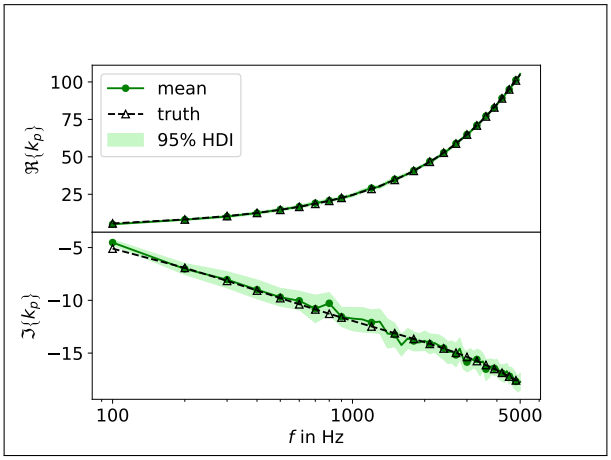

Figure 3. Posterior mean (solid green with dots), its associated 95 % highest posterior density interval (HDI, green shaded), and the ground truth (black dashed with triangles) of the sought wavenumber.

Fig. 5 presents the oblique incidence sound absorption coefficient of the panel absorber, including its associated uncertainty. Three different incidence angles are

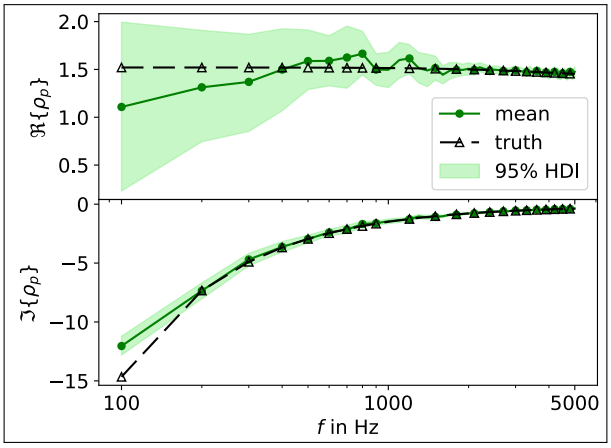

Figure 4. Posterior mean (solid green with dots), its associated 95 % highest posterior density interval (HDI, green shaded), and the ground truth (black dashed with triangles) of the sought effective density.

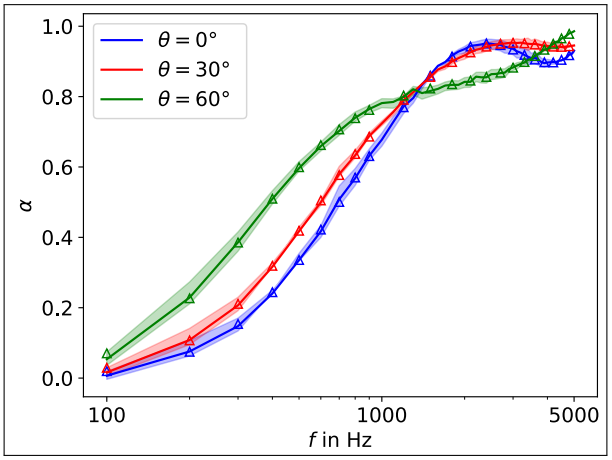

Figure 5. Posterior mean (solid), 95 % highest density interval (shaded) and ground truth (triangles) of the oblique incidence plane wave sound absorption coefficient α for three angles of incidence θ.

investigated: Normal incidence ($\theta = 0°$), an incidence angle of $\theta = 30°$, and $\theta = 60°$. It becomes clear that the absorption behavior of the panel absorber changes significantly with the angle of incidence. Yet, the posterior mean of the absorption coefficient matches with the ground truth for all angles of incidence due to the accurately inferred sound propagation characteristics. Notably, this approach enables an accurate estimation of the sound absorption coefficient even for larger angles of incidence than those analyzed with the measurement setup. Regarding the uncertainty in the absorption coefficient, it is of comparable magnitude for all angles of incidence and is particularly low in the range of 400–1600 Hz for normal incidence and for $\theta = 30°$ and for frequencies above 4500 Hz for all angles of incidence.

5. DISCUSSION

This concept study shows that it is possible to estimate the oblique incidence sound absorption coefficient and the associated uncertainty inherent in the measurement process. The required data stem from simulated free-field impedance measurements using a virtual source antenna and a PU-probe. Although the initial results are promising, there are some challenges to applying this method in an actual experimental application. First, the bounds for the prior probabilities need to be cautiously specified, particularly for those parameters, which are not restricted by physical constraints, *i.e.* the upper bound of the real part and the lower bound of the imaginary part of the wavenumber. Second, the inference is challenging due to a potentially multimodal posterior. Consequently, convergence at a discrete frequency cannot be guaranteed with a very small sample size, even though the inference starts in a region of high probability. For this reason, the number of samples in the sequential phase needs to be higher compared to the direct inference of the surface admittance presented in Ref. [6]. This leads to an increase in the total computational runtime. Third, this concept study deals only with data from simulated experiments. As such, the framework needs to be validated against true measurements, where the directivity of the PU-probe varies with the angle of incidence, and particular attention must be paid to using sufficiently large samples to avoid edge diffraction effects while guaranteeing enough space for the source trajectory.

Future work aims at speeding up the inference process by using more elaborate selection strategies of the discrete frequencies. From a practical point of view, future research will address the application of the proposed framework to a more convenient measurement setup, *e.g.* using a single stationary loudspeaker and a microphone array, and the validation of the proposed method against real experimental data.

6. ACKNOWLEDGMENTS

Eric Brandão would like to thank the National Research Council of Brazil (CNPq - Conselho Nacional de Desenvolvimento Cientifico e Tecnologico) for the partial financial support to this research paper (Projeto Universal: n° 402633/2021-0).

7. REFERENCES

[1] "Iso 10534–2: Acoustics - determination of sound absorption coefficient and impedance in impedance tubes - part 2: Transfer-function method," International Organization for Standardization, Geneva, Switzerland, 2001.

[2] H.-S. Tsay and F.-H. Yeh, "The influence of circumferential edge constraint on the acoustical properties of open-cell polyurethane foam samples," *The Journal of the Acoustical Society of America*, vol. 119, no. 5, pp. 2804–2814, 2006.

[3] E. Brandão, A. Lenzi, and S. Paul, "A review of the in situ impedance and sound absorption measurement techniques," *Acta Acustica united with Acustica*, vol. 101, no. 3, pp. 443–463, 2015.

[4] M. Alkmim, J. Cuenca, L. De Ryck, and W. Desmet, "Angle-dependent sound absorption estimation using a compact microphone array," *The Journal of the Acoustical Society of America*, vol. 150, no. 4, pp. 2388–2400, 2021.

[5] S. Dupont, M. Sanalatii, M. Melon, O. Robin, A. Berry, and J.-C. Le Roux, "Characterization of acoustic materials at arbitrary incidence angle using sound field synthesis," *Acta Acustica*, vol. 6, p. 61, 2022.

[6] M. Eser, S. Mannhardt, C. Gurbuz, E. Brandão, and S. Marburg, "Free-field characterization of locally reacting sound absorbers using bayesian inference with sequential frequency transfer," submitted to Mechanical Systems and Signal Processing.

[7] M. Eser, C. Gurbuz, E. Brandão, and S. Marburg, "Direct discrete complex image method for sound field evaluation above a non-locally reacting layer," *The Journal of the Acoustical Society of America*, vol. 150, no. 5, pp. 3509–3520, 2021.

[8] K. M. Li, T. Waters-Fuller, and K. Attenborough, "Sound propagation from a point source over extended-reaction ground," *The Journal of the Acoustical Society of America*, vol. 104, no. 2, pp. 679–685, 1998.

[9] J. Allard, W. Lauriks, and C. Verhaegen, "The acoustic sound field above a porous layer and the estimation of the acoustic surface impedance from free-field measurements," *The Journal of the Acoustical Society of America*, vol. 91, no. 5, pp. 3057–3060, 1992.

[10] J. F. Allard and N. Atalla, *Propagation of Sound in Porous Media*. John Wiley & Sons, Ltd, 2009.

[11] H. de Bree, "An overview of microflown technologies," *Acustica united with Acta Acustica*, vol. 89, no. 1, pp. 163–172, 2003.

[12] R. M. Neal, "Slice sampling," *The Annals of Statistics*, vol. 31, no. 3, pp. 705–767, 2003.

[13] P. Del Moral, A. Doucet, and A. Jasra, "Sequential monte carlo for bayesian computation," in *Bayesian Statistics 8* (J. M. Bernardo, M. J. Bayarri, J. O. Berger, A. P. Dawid, D. Heckerman, A. F. M. Smith, and M. West, eds.), pp. 1–34, Oxford University Press, 2007.